

PACS numbers: 42.55.Lt; 42.60.Jf; 42.60.Lh
DOI: 10.1070/QE2008v038n09ABEH013516

Study of a helium laser pumped by a pulsed electron beam generated in an open discharge

E.V. Bel'skaya, P.A. Bokhan, Dm.E. Zakrevskii

***Abstract*. A laser on the self-contained helium $2^1P_1^0 - 2^1S_0$ transition pumped by a pulsed electron beam generated in an open discharge is simulated and experimentally studied. Lasing without decreasing the pulse energy in a tube of diameter 31 mm was observed up to the pump pulse repetition rate of 10 kHz determined by the parameters of a power supply. Dynamics of the electric field in an accelerating gap and populations of the working levels of helium are calculated. The radiation power calculated in accordance with its radial distribution measured in the saturated amplification regime is 7.85 times higher than that in the lasing regime. The practical laser efficiency of 0.056 % is achieved for the quantum efficiency of 0.7 %.**

Keywords: *helium laser, open discharge, electron beam.*

1. Introduction

Self-contained atomic transition lasers belong to the most powerful and efficient lasers in the visible spectral region. They are especially promising upon pumping by kilo-electron-volt electron beams generated in an open discharge. In particular, the average power of up to 10 kW m^{-1} was predicted for copper-vapour lasers [1]. However, to achieve such parameters, it is necessary to solve a number of scientific and technical problems, of which the main are:

(i) Generation of pulsed nanosecond $\sim$ 10-kA, 5-keV electron beams with the efficiency η_e of no less than 0.9 at high repetition rates.

(ii) Study of the self-contained laser (SCL) kinetics at a high pump level accompanied by considerable superradiance losses in non-axial beams.

The simplest representative of SCLs is a helium laser emitting at the transition from the resonance $2^1P_1^0$ state to the metastable 2^1S_0 state at 2058.3 nm. Helium is one of most thoroughly studied atoms for which numerous data on constants and cross sections of elementary processes involving electrons and heavy particles have been obtained. The properties of a helium laser can be further used to develop other gas lasers having a large practical importance but for which data on rates of elementary processes are absent. In addition, a helium laser turned to be an efficient tool for studying fundamental processes in a gas discharge [2].

Earlier superradiance was obtained in a gas-discharge helium laser under extreme conditions, namely, voltage amplitude up to 50 kV in a tube of diameter 1.3 mm and length 200 mm [3]. Upon pumping in an open discharge, generation and superradiance were observed at rather modest electron-beam parameters (5 kV, 100 A) [4].

In this paper, we simulated and studied experimentally a He laser with the working channel of diameter 31 mm, which allows the electron beam energy to be used completely. The laser parameters were measured both in the lasing and saturated amplification regimes. The field dynamics in the accelerating gap of the open discharge and energy parameters of the laser were calculated and compared with the experimental data.

2. Experimental setup

Experiments were mainly performed by using a coaxial laser cell [5]. To increase the stability of the open-discharge burning, a metal-ceramic cathode [6] with the internal diameter $d_c = 33$ mm was used, to which pulsed negative voltage was applied. A metal grid with the geometrical transparency $\mu = 0.64$ and the characteristic cell size of 0.3 mm, which was rolled up in a cylinder of diameter $d_a = 31$ mm and grounded through the current-measuring shunt with $R = 0.3\ \Omega$, played the role of the anode. The length l of the working part of the laser cell was 120 mm. The electron beam was generated in the accelerating gap of length 1 mm between the cell cathode and anode, while radiation was generated in the drift space behind the anode. The optical resonator was formed by a highly reflecting mirror on one side and by a plane – parallel plate on the other side. Output windows were mounted at an angle of 20° to the resonator axis. A TGI1-1000/25 thyratron with the storage capacity of $C = 8$ nF and peaking capacity of $C_0 = 6.6$ nF was used as a switch in the generator of the laser pulsed power supply.

A master oscillator – power amplifier system was used to study the amplifying properties of the laser. The laser cell of the master oscillator also pumped by an electron beam was a coaxial cell with a metal cathode of diameter $d_c = 17.2$ mm, an anode in the form of a metal grid with $d_a = 15.2$ mm,

E.V. Bel'skaya, P.A. Bokhan, Dm.E. Zakrevskii Institute of Semiconductor Physics, Siberian Branch, Russian Academy of Sciences, prosp. Akad. Lavrent'eva 13, 630090 Novosibirsk, Russia; e-mail: zakrdm@isp.nsc.ru

Received 28 December 2006; revision received 13 June 2007
Kvantovaya Elektronika **38** (9) 823 – 828 (2008)
Translated by I.A. Ulitkin

$l = 90$ mm, $C = 4.7$ nF and $C_0 = 3.3$ nF. The working capacity of the master oscillator was switched by the same thyratron as the storage capacity of the power amplifier. The pump pulses of the master oscillator and power amplifier were shifted within 325 ns by introducing inductances in the power supply circuit.

The $He:N_2 = 99.1:0.9$ gas mixture was used as the working mixture. The optimal pressure of He (depending on the working voltage and the mixture composition) was 15–30 Torr. The nitrogen provided better discharge stability, increased the rate of its development and lasing energy as well as participated in the depopulation of the lower working level. The deexcitation rate constants of the helium level 2^1S_0 by the nitrogen molecules and electrons were 6.9×10^{-11} and 4.2×10^{-9} cm^3 s^{-1}, respectively [7]. For the typical working parameters of the laser, the rates of deexcitation processes for the metastable state were $A_h = 3.42 \times 10^5$ s^{-1} in collisions with nitrogen and $A_e = 1.75 \times 10^5$ s^{-1} in collisions with electrons.

3. Experimental results

3.1 Lasing regime

Our studies showed that the laser accelerating gap had pronounced peaking properties. Figure 1 presents the oscillograms of the voltage between the anode and cathode of the power amplifier and the discharge current at helium and nitrogen pressures of $P_{He} = 16$ Torr and $P_{N_2} = 0.15$ Torr. One can see that the duration of the current pulse through the accelerating gap is almost an order of magnitude smaller that the duration of the current through the thyratron, while its amplitude is correspondingly higher, which substantially simplifies the switch operation.

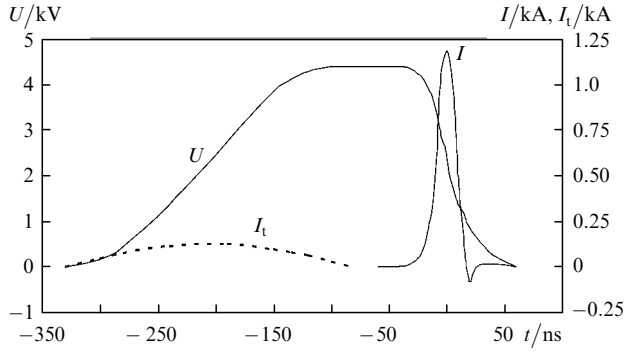

Figure 1. Oscillograms of the voltage U on the cathode, discharge current I in the laser accelerating gap and current I_t through the thyratron.

Figure 2 shows the dependences of the current amplitude I_{max} through the acceleration gap, the reduced lasing power P_{las} and the lasing efficiency η_{las} with respect to the energy stored in the peaking capacitor C_0 on the accelerating voltage amplitude U_g for the same values of P_{He} and P_{N_2}. In the range of voltages and working pressures (15–30 Torr) under study, the lasing energy and current amplitude are independent of the pulse repetition rate F in the region from 1 to 10 kHz (the upper limit F is limited by the power supply parameters). For $F < 1$ kHz a gradual decrease in the lasing energy is observed, which is caused by

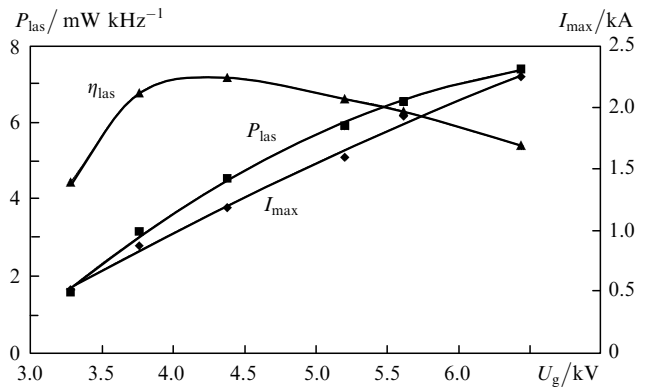

Figure 2. Dependences of the current amplitude I_{max}, the reduced lasing power P_{las} and the lasing efficiency η_{las} with respect to the energy stored in C_0 on the amplitude of the accelerating voltage U_g on the cathode.

a decrease in the current amplitude. For the constant current amplitude achieved by an insignificant increase in the working voltage, the lasing energy did not change at $F < 1$ kHz. One can see from Fig. 2 that in the voltage region from 3.75 to 5 kV, the value of η_{las} was almost independent of U_g, therefore, studies below were performed at $U_g = 4.4$ kV.

3.2 Oscillator – amplifier system

To study the amplifying properties, the beam from the master oscillator was compressed in a telescope to a diamater of 5 mm and directed to the power amplifier. The central part of the radiation was separated by the 1.6-mm aperture. The optical system allowed scanning the beam from the master oscillator over the entire cross section of the power amplifier. Figure 3 presents the dependence of the reduced lasing power density p_{las}^{PA} and the photon density N_{ph}^{PA}, equal to it with the accuracy to a coefficient, at the output from the power amplifier on the lasing power density of the master oscillator. One can see that the saturated amplification regime is achieved for the lasing power density of the master oscillator equal to 2 mW kHz^{-1}cm^{-2}, which corresponds to $N_{ph} = 2 \times 10^{13}$ cm^{-2}. Figure 4 illustrates the dependence of p_{las}^{PA} at

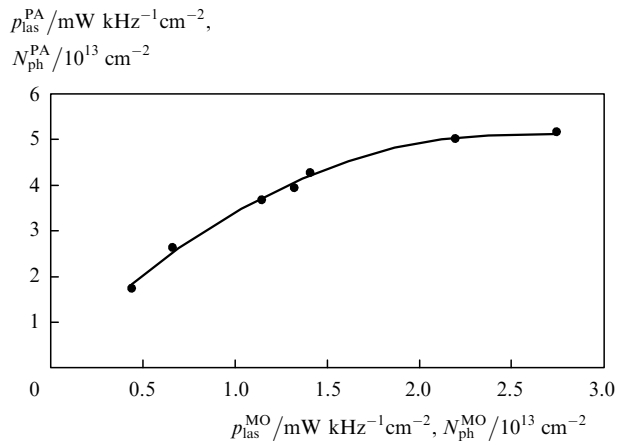

Figure 3. Dependence of the reduced lasing power density p_{las}^{PA} and the photon density N_{ph}^{PA} at the power amplifier output on p_{las}^{MO} of the master oscillator radiation (N_{ph}^{MO}).

the power amplifier output on the temporal shift $\Delta\tau$ of pump pulses of the master oscillator with respect to the power amplifier. For $\Delta\tau = 0$ the system operates in the regime of optimal synchronisation, while for $\Delta\tau < 0$ the oscillator pump pulse precedes the amplifier pump pulse. The master oscillator radiation was transmitted at a distance of 1 cm from the amplifier axis. Thus, the work of the peripheral part of the power amplifier cell was studied. The development of the superradiance in the amplifier prevented measurement of this dependence in the central region of the tube. The lasing power density of the master oscillator equal to 1.2 mW kHz^{-1}cm^{-2} corresponds to the zero power density at the power amplifier output. For $\Delta\tau \approx 150 - 200$ ns, the power amplifier working medium is bleached, which is caused by the relaxation of the metastable state in the afterglow.

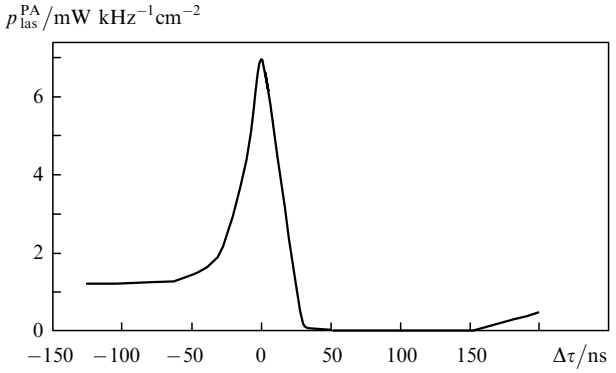

Figure 4. Dependence of the reduced lasing power density p_{las}^{PA} at the power amplifier output on the time shift $\Delta\tau$ of pump pulses of the master oscillator with respect to the power amplifier.

Figure 5 shows the relative distribution of the reduced lasing power density in the cross section of the power amplifier tube in the lasing and amplification regimes. Upon integration in the entire cross section, the reduced lasing power P_{max} in the saturated amplification regime is 35.6 mW kHz^{-1} and in the lasing regime is $P_{las} =$ 4.5 mW kHz^{-1}. When pure helium (without nitrogen) is used, the values of η_{las} and P_{las} are, as a rule, 1.5 times smaller, while the optimal working pressure is two times higher than that in the mixture of helium with nitrogen.

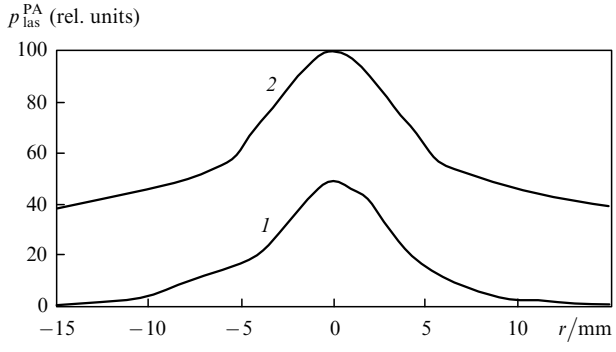

Figure 5. Radial distributions of the reduced lasing power p_{las}^{PA} at the power amplifier output in the lasing (*1*) and amplification (*2*) regimes.

4. Simulation of the laser

4.1 Methods for calculating the distribution of the electric field strength and potential in the accelerating gap in the open discharge

To calculate the energy characteristics of the laser, it is necessary to know information about the spectrum of fast electrons in the electron beam. First of all, it is required to determine the potential distribution $U(x,t)$ in the accelerating gap, which can be calculated from the system of equations

$$\frac{\mathrm{d}U(x,t)}{\mathrm{d}x} = E(x,t),$$

$$\frac{\mathrm{d}E(x,t)}{\mathrm{d}x} = \frac{4\pi}{\varepsilon_0}\frac{j_i(x,t) - j_i(x,t-\Delta t)}{v_i}, \qquad (1)$$

$$\frac{\mathrm{d}j_i(x,t)}{\mathrm{d}x} = -j_e(t)\frac{\theta K}{w_0}\gamma(w) - \int_0^x \frac{\theta K}{w_0}\gamma(w)\frac{\partial j_i(x_1,t)}{\partial x_1}\mathrm{d}x_1$$

under boundary conditions

$$U(0,t) = -|U(t)|, \quad \int_0^L E(x,t)\mathrm{d}x = |U(0,t)|, \quad j_i(L,t) = 0,$$

where $E(x,t)$ is the electric field strength in the accelerating gap; $j_i(x,t)$, $j_i(x,t-\Delta t)$ are the current densities of ions produced in the accelerating gap in this and previous iterations in time, respectively;

$$\gamma(w) = 1.87 \times 10^4\left[1 - \exp\left(-\frac{w-41.3}{229.5}\right)\right]\frac{\ln w}{w}$$

is the stopping power of helium obtained by approximating data [8], in MeV cm^{2}g^{-1}; $v_i = a\sqrt{E(x,t)}$ is the drift ion velocity approximated according to experimental data [9, 10] (in this paper, $a = 8$); $j_e(t)$ is the current density of the electron beam through the accelerating gap; $I(t)$ and $U(t)$ are the experimental values of the discharge current and voltage on the cathode; $\theta = 0.6$ is the energy fraction of fast electrons spent on ionisation [11, 12]; $K = 1.4$ is the coefficient taking into account angular scattering of fast electrons in a strong external field [13]; $w_0 = 50$ eV is the energy spent on production of one helium ion [12]; $w = e[U(x,t) - U(0,t)]$ is the energy acquired by an electron after passage through the potential difference. The coordinate $x = 0$ corresponds to the cathode, L is the length (along the x axis) of the cathode potential drop. It was obtained experimentally that under the open discharge conditions in the region of average helium pressures up to hundreds of Torr, $\eta_e = j_e/j \approx 1$ [13] [j is the density $I(t)$ of the discharge current being measured in the accelerating gap], which allows one to set the density $j_e(t)$ equal to the density of the discharge current being measured in the accelerating gap. The expression for the ion current density is written in accordance with paper [13].

The algorithm of the numerical solution was as follows: for functions $U(x,t)$, $E(x,t)$, $j_i(x,t)$ and $v(x,t) = \mathrm{d}j_i(x,t)/\mathrm{d}x$, system (1) was rewritten into a system of differential equations, which was solved separately at each instant t with the initial conditions $U(0,t) = -|U(t)|$, $E(0,t) = A$,

$j_i(0,t) = B$, $v(0,t) = 0$, where A and B are the fitting parameters selected to fulfill the boundary conditions. For $t = t_{min}$, we have $j_e(t) = 0$, the potential $U(x,t)$ is distributed linearly, the field $E(x,t)$ – uniformly. By solving equations in one iteration, functions $U(x,t)$ and $E(x,t)$ are found at the instant t, in the next iteration – at the instant $t + \Delta t$. The potential $U(x,t)$ and the field $E(x,t)$ at the end of the current pulse are determined through $T/\Delta t$ of iterations from the beginning of calculations, where T is the total pulse duration of the discharge current $I(t)$. The time interval Δt was selected so that when it decreased, the distributions $U(x,t)$ and $E(x,t)$ did not change at the end of the current pulse.

In paper [13] the field potential in the accelerating gap of length 1 mm was measured by the probe method. In particular, the amplitude dependence was obtained for rise time constant t_0 of the current increasing by e times through the gap and the current density of the potential cutoff j_{cf} on the probe located at a distance of 0.2 mm from the cathode for $P_{He} = 30$ Torr. The cutoff current is the current in the accelerating gap for which the potential at the probe is zero.

Figure 6 presents the measured and calculated values of j_{cf} for $L = 0.24$ mm (thus, the finite probe diameter was taken into account) for different U_g. The difference between the theoretical and experimental values of j_{cf} at large t_0 is explained by the fact that system of equation (1) neglects the flow of ions on the cathode. One can see that for $t_0 = 29$ ns the calculated and experimental values of j_{cf} coincide. This means that at these times of the discharge development the ion current on the cathode can be neglected in calculations of the potential distribution in the accelerating gap, which significantly simplifies the calculation.

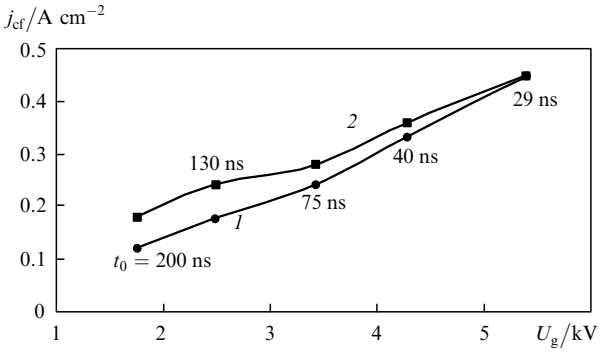

Figure 6. Theoretical (*1*) and experimental (*2*) values of the densities of the potential cutoff current j_{cf} at a distance of 0.24 mm from the cathode for different values of the time constant t_0 of the current increasing by e times through the gap and voltage amplitudes U_g on the cathode.

4.2 Field dynamics in the laser acceleration gap

By using system of equations (1), we calculated the potential $U(x,t)$ and the field strength $E(x,t)$ in the accelerating gap under the following optimal conditions: $P_{He} = 16$ Torr, $P_{N_2} = 0.15$ Torr; $U_g = 4.4$ kV, $I_{max} = 1.2$ kA. The values of the potential on the cathode and discharge current at different instants were taken from experimental oscillograms (Fig. 1). Up to 0.9 kA, the oscillogram of the current in the accelerating gap is approximated by the exponential $I(t) = I_0 \exp(t/t_0)$ with a high accuracy, where $t_0 = 6.5$ ns. The calculation of the spatiotemporal field distribution in the laser gap by using system of equations (1) can be assumed valid because $t_0 = 6.5$ ns $\ll 29$ ns. Figure 7 presents the results of calculations and Fig. 8 shows the stretched oscillograms of the voltage $U(t)$ on the cathode and the discharge current $I(t)$ with the time scale corresponding to the calculations. In the absence of the discharge current, the potential on the anode is $U(L) = 0$, $E(x) = \text{const}$ along the length of the accelerating gap. The field strength on the cathode increases with time and the length of the region of the cathode potential fall decreases occupying only a part of the accelerating gap. For the maximal current (Fig. 8, $t = 0$) the field is concentrated at a distance of 0.078 mm from the cathode, which corresponds to the reduced field strength on the cathode $E/N = 1.14 \times 10^5$ Td (1 Td = 10^{-17} V cm^2). For this values of E/N, η_e exceeds 0.95 [13] and the electron beam propagated through the anode grid is almost monoenergetic at each instant with the energy equal to $eU(t)$, where $U(t)$ is the potential on the cathode.

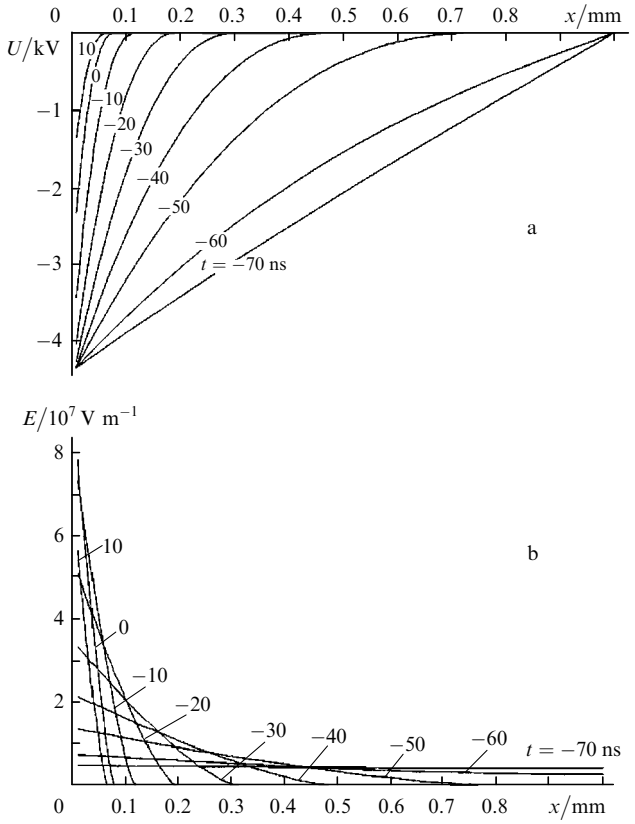

Figure 7. Distribution of the potential $U(x,t)$ and electric field strength $E(x,t)$ in the laser accelerating gap. The moment of the current maximum establishment is taken for $t = 0$.

4.3 Energy parameters of the laser

The electron beam energy spent on excitation and ionisation of helium atoms in the drift space is calculated from the initial energy of electrons propagated through the grid anode and energy losses spent on the deceleration of the electron beam on the atoms due to inelastic collisions. The electron beam power P_e supplied to the laser active medium is calculated from the relation $P_e = WI(t)\mu$, where W is the

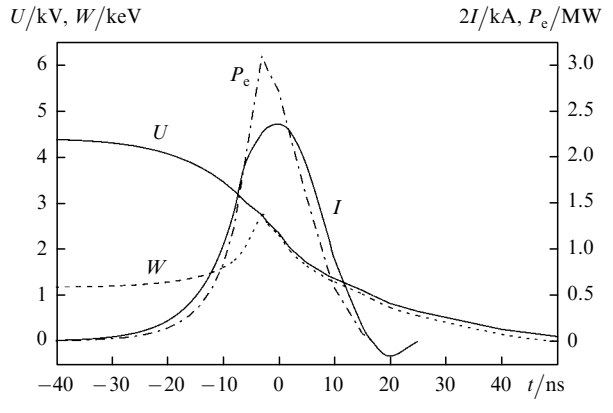

Figure 8. Time dependences of the voltage U on the cathode, the discharge current I in the accelerating gap as well as the energy W per electron supplied in the drift space and the electron beam power P_e.

energy per electron used to ionise and excite He atoms in the drift space. Figure 8 presents the time dependences of U, W, I, P_e.

The total number of ions and the populations of the resonance and metastable atomic states were calculated from the equations

$$\frac{dN_{rs}^{st}}{dt} = \frac{P_e}{\varepsilon_{rs}}\eta_{rs}, \quad \frac{dN_{ms}^{st}}{dt} = \frac{P_e}{\varepsilon_{ms}}\eta_{ms}, \quad \frac{dN_i}{dt} = \frac{P_e}{\varepsilon_i}\eta_i, \tag{2}$$

where N_{rs}^{st}, N_{ms}^{st} is the total number of He atoms excited in the resonance and metastable states, respectively; N_i is the number of ions in the entire laser volume; $\varepsilon_i = 24.6$ eV, $\varepsilon_{rs} = 21.2$ eV, $\varepsilon_{ms} = 20.6$ eV are the energies spent on ionisation and excitation of helium resonance and metastable states, respectively; $\eta_i = 0.602$, $\eta_{rs} = 0.181$, $\eta_{ms} = 0.027$ are the electron beam energy fractions spent on ionisation and excitation of the helium resonance and metastable states [11]. In the saturated power approximation, the system of equations

$$N_{rs}^{st} + N_{ms}^{st} = N_{rs}^{f} + N_{ms}^{f}, \quad N_{rs}^{f} = N_{ms}^{f}\, g_{rs}/g_{ms} \tag{3}$$

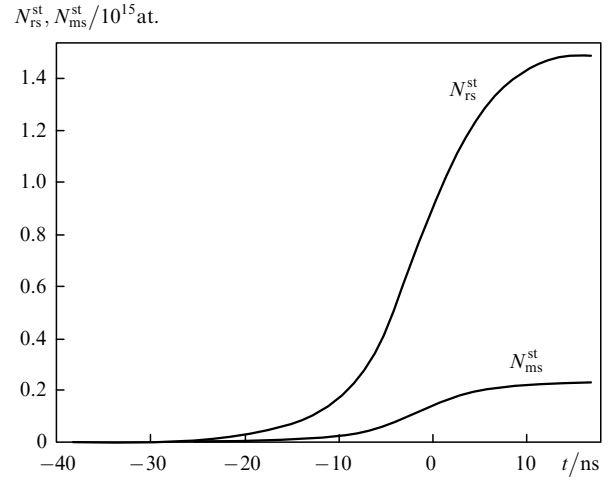

Figure 9. Time dependences of the numbers of excited He atoms total by the laser volume in the resonance (N_{rs}^{st}) and metastable (N_{ms}^{st}) states of helium.

is valid, where $g_{rs} = 3$, $g_{ms} = 1$ are the statistical weights of the resonance and metastable states; subscripts st and f correspond to the values of populations before and after lasing. The fraction of nitrogen in the working mixture was less than one percent. This amount of N_2 cannot significantly decrease the energy supplied to helium and, hence, the presence of nitrogen in calculations of the lasing power was not taken into account. The time dependences of the total number of helium atoms excited to the working levels (by neglecting the stimulated emission) are presented in Fig. 9.

The population inversion over the entire volume and calculated from (2) is $N_{rs}^{st} - (g_{rs}/g_{ms})N_{ms}^{st} = 8.04 \times 10^{14}$. The lasing power is $P_{theor} = (N_{rs}^{st} - N_{rs}^{f})h\nu = 19.4$ mW kHz^{-1}, where $h\nu$ is the quantum energy. The high concentration of electrons (4.16×10^{13} cm^{-3}) along with the presence of nitrogen provides fast relaxation of metastable states in the afterglow with the rate $A_\Sigma = A_h + A_e = 5.16 \times 10^5$ s^{-1}.

5. Discussion of the results

The lasing power $P_{las} = 4.5$ mW kHz^{-1} was obtained in the experiment for $P_{He} = 16$ Torr, $P_{N_2} = 0.15$ Torr, $U_g = 4.4$ kV and $I_{max} = 1.2$ kA. The power P_{theor} calculated for the same parameters was equal to 19.4 mW kHz^{-1}. The possible reasons for the difference between the theoretical and experimental results can be caused either by the presence of emission in the nonaxial directions due to the noticeable reflectance from the tube walls or by the discrepancy of the real distribution of the pump power over the He states calculated theoretically, or by the influence of nitrogen atoms on the degradation spectrum of electrons. The nonsaturated gain of He atoms due to Doppler broadening is $k_0 = 1.69 \times 10^{-12}(N_{rs}^{st}/g_{rs} - N_{ms}^{st}/g_{ms})g_{rs}/V$. Then, the amplification at the length equal to the tube diameter is $\exp(k_0 d_a) = 7.8 \times 10^{17}$, which can undoubtedly lead to lasing in non-axial directions.

To determine the contribution of possible radiation losses in non-axial directions, consider the results of investigation of the oscillator–amplifier system. The comparison of radial distributions of the laser power density in the lasing and amplification regimes (see Fig. 5) shows that not all population inversion is removed in the lasing regime on the laser cell axis – the peripheral part of the cell operates only in the amplification regime. The lasing power $P_{max} = 35.6$ mW kHz^{-1}, calculated according to its measured radial distribution in the saturated amplification regime exceeds by 7.9 times the power P_{las} obtained in the lasing regime. The discrepancy between P_{max} and P_{theor} can be caused both by technical reasons (inaccuracy of experimental measurements) and by physical reasons, in particular, by changes in the degradation spectrum of electrons due to addition of nitrogen to the working medium. The results of studies of a laser with the active medium without nitrogen are in favour of the last assumption. In this case, the lasing power is approximately 1.5 times lower and close to the calculated one.

The lasing efficiency in the amplification regime η_{las}^{PA} with respect to the energy stored in the peaking capacitor C_0 was 0.056 %. The consideration of losses on the grid and incomplete deceleration of the electron beam in the initial stage of the discharge till the time $t = -3$ ns according to Fig. 8 (the latter decreases the energy supplied to the tube by

23.5 %) yields the lasing efficiency $\eta_{max} = \eta_{las}^{PA}[(1-0.235)\mu]^{-1} = 0.115\,\%$ of the supplied energy, which is 0.16 of the quantum efficiency of the working transition equal to 0.7 %.

6. Conclusions

We have shown that, by using metal-ceramic cathodes in the open discharge, stable generation of high-power electron beams with a high repetition rate can be obtained. This allows one to obtain the superradiance regime of a helium self-contained laser already in comparatively short tubes. In the experiments performed, the laser radiation pulse energy did not decrease till the pump pulse repetition rate of 10 kHz, which confirms the efficiency of using an electron beam generated in the open discharge to pump SCLs.

Calculation of the electric field dynamics in the accelerating gap has shown that the generated beam is virtually monoenergetic, which simplifies the simulation of the laser. The comparison of calculated and measured lasing parameters in the saturated amplification regime revealed their proximity for a He laser whose active medium does not contain nitrogen. The output power obtained in $He - N_2$ mixtures is 1.8 times higher than the calculated power, which can be explained by the influence of N_2 on the degradation spectrum of electrons and by a change in the partial contributions of the electron beam power to the excitation of the working helium levels. The achieved laser efficiency equal to 16 % of the quantum efficiency suggests that electron beams are promising for pumping SCLs.

Acknowledgements. This work was partially supported by the Russian Foundation for Basic Research (Grant No. 06-08-00272).

References

1. Bokhan P.A., Molodukh E.I. *Pulsed Metal Vapour Lasers* (Dortrecht – Boston – London: Kluwer Acad. Publ., 1996) Vol. 5, p. 137.
2. Bokhan P.A., Zakrevskii D.E. *Zh. Tekh. Fiz.*, **77**, 109 (2007) [*Technical Physics*, **52**, 104 (2007)].
3. Isaev A.A., Ishchenko P.I., Petrash G.G. *Pis'ma Zh. Eksp. Teor. Fiz.*, **6**, 619 (1967).
4. Bokhan P.A., Sorokin A.R. *Pis'ma Zh. Tekh. Fiz.*, **2**, 947 (1982).
5. Bokhan P.A. *Entsiklopedia nizkotemperaturnoi plazmy* (Encyclopedia of a Low-Temperature Plasma) (Moscow: Fizmatlit, 2005) Ser. B, Vol. X1-4, p. 316.
6. Bokhan P.A., Zakrevskii D.E., Mali V.I., Shevnin A.M., Yancharina A.M. *Kvantovaya Elektron.*, **16**, 1110 (1989) [*Sov. J. Quantum Electron.*, **19**, 719 (1989)].
7. Newman L.A. *IEEE J. Quantum Electron.*, **17**, 1182 (1981).
8. La Verne J., Mozumder A. *J. Phys. Chem.*, **89**, 4219 (1985).
9. Helm H. *J. Phys. B: Atom. Molec. Phys.*, **10**, 3683 (1977).
10. Rundel R.D., Nitz D.E., Smith K., Genis M.W., Stebbings R.F. *Phys. Rev. A*, **19**, 33 (1979).
11. Sytsko Yu.N., Yakovlenko S.I. *Fiz. Plazmy*, **2**, 63 (1976).
12. Arlantsev S.V., Borovich B.L., Buchanov V.V., Molodykh E.I., Yurchenko N.I. *J. Rus. Laser Research*, **16**, 99 (1995).
13. Bokhan A.P., Bokhan P.A., Zakrevskii D.E. *Fiz. Plazmy*, **32**, 599 (2006) [*Plasma Physics Reports*, **32**, 549 (2006)].